© 2022. Published by The Company of Biologists Ltd | Development (2022) 149, dev199984. doi:10.1242/dev.199984

RESEARCH ARTICLE

Smad4 controls proliferation of interstitial cells in the neonatal kidney

Sarah S. McCarthy[1], Michele Karolak[1] and Leif Oxburgh[2,*]

ABSTRACT

Expansion of interstitial cells in the adult kidney is a hallmark of chronic disease, whereas their proliferation during fetal development is necessary for organ formation. An intriguing difference between adult and neonatal kidneys is that the neonatal kidney has the capacity to control interstitial cell proliferation when the target number has been reached. In this study, we define the consequences of inactivating the TGFβ/Smad response in the mouse interstitial cell lineage. We find that pathway inactivation through loss of *Smad4* leads to overproliferation of interstitial cells regionally in the kidney medulla. Analysis of markers for BMP and TGFβ pathway activation reveals that loss of Smad4 primarily reduces TGFβ signaling in the interstitium. Whereas TGFβ signaling is reduced in these cells, marker analysis shows that Wnt/β-catenin signaling is increased. Our analysis supports a model in which Wnt/β-catenin-mediated proliferation is attenuated by TGFβ/Smad to ensure that proliferation ceases when the target number of interstitial cells has been reached in the neonatal medulla.

KEY WORDS: Smad, TGFβ, Wnt, Mouse

INTRODUCTION

Interstitial cells are any cells located between the functional cells, or parenchyma, of a tissue. In the kidney, cells of the nephron and blood vessel are considered the functional components and the interstitial cell population is made up largely of PDGFRβ-expressing fibroblasts. These cells derive from a *Foxd1*-expressing progenitor, which also gives rise to mesangial cells, the specialized pericytes of the glomerulus. Expansion of interstitial cells in the adult kidney is a hallmark of chronic disease, with unopposed interstitial cell proliferation leading to progressive scarring (fibrosis) and concomitant loss of parenchyma (Humphreys et al., 2010). In contrast, proliferation of interstitial cells plays an essential role in fetal development and somatic growth of the kidney (Boivin and Bridgewater, 2018; Das et al., 2013; Fetting et al., 2014; Hatini et al., 1996). An intriguing difference between adult and neonatal kidneys is that the neonatal kidney has the capacity to control interstitial cell proliferation when the target number has been reached, and our study aims to characterize the basic mechanisms of this proliferation control.

Gene inactivation and experimental therapeutics targeting the TGFβ signaling pathway have been used to reduce fibrosis in kidney injury models (Inazaki et al., 2004; Morishita et al., 2014), indicating that the pathway is a significant driver of interstitial expansion. We therefore hypothesized that the TGFβ pathway may control interstitial cell proliferation in the neonatal kidney. Although TGFβ signaling has been a focus of research in homeostasis of adult interstitial cells, little is known about its function in differentiation of the renal interstitium. TGFβ signaling is essential for development of the kidney (Dudley et al., 1995; Ikeya et al., 2010; Oxburgh et al., 2004), and controls formation of both the collecting ducts and nephrons (Brown et al., 2013; Hartwig et al., 2008). Recessive mutations in genes within this signaling pathway have been identified as monogenic causes of congenital anomalies of the kidney and urinary tract (CAKUT), indicating that TGFβ pathway dysregulation may be an important factor in neonatal kidney disease. An important example is the identification of mutations in bone morphogenetic protein 4 (BMP4) in patients with renal hypodysplasia (Kohl et al., 2014; Weber et al., 2008).

TGFβ superfamily ligands signal through two distinct intracellular pathways: the Smad pathway, which is initiated by phosphorylation of receptor-associated Smad (R-Smad) transcription factors, and the mitogen-associated protein kinase (MAPK) pathway, which is initiated by the TGFβ-associated kinase MAP3K7 (also known as TAK1). Kidneys of mice with conditional inactivation of *Map3k7* in the *Foxd1* lineage develop spontaneous neonatal mesangiosclerosis (Karolak et al., 2018), suggesting that MAPK is selectively required for mesangial differentiation.

The current study addresses the role of Smad pathway signaling in the *Foxd1* lineage. Phosphorylated R-Smads associate with the common mediator Smad (Smad4) to accumulate in the nucleus. R-Smads and Smad4 bind DNA and interact with a variety of other transcription factors, facilitating highly context-dependent responses. Because Smad4 is unique and essential for Smad-mediated responses, we selected it as a tractable node in the pathway for conditional gene inactivation. We report that *Smad4* controls proliferation within the interstitium of the mouse neonatal kidney by attenuating Wnt signaling.

RESULTS

Loss of Smad4 causes expansion of the renal interstitium

To understand the role of TGFβ/BMP in the developing renal interstitium, *Smad4* was inactivated in interstitial cell progenitors using $Foxd1^{Cre}$. To sensitize the strain for Cre-mediated recombination, $Foxd1^{Cre}$ was combined with one null *Smad4* allele and one loxP-flanked allele (Chu et al., 2004). This cross generates offspring of four genotypes: $Foxd1^{+/+}$;$Smad4^{-/loxp}$, $Foxd1^{+/+}$;$Smad4^{+/loxp}$, $Foxd1^{+/Cre}$;$Smad4^{+/loxp}$ and $Foxd1^{+/Cre}$;$Smad4^{-/loxp}$. *Foxd1* is disrupted in the $Foxd1^{cre}$ strain and $Foxd1^{+/Cre}$;$Smad4^{+/loxp}$ was selected as the control group (referred to as $Smad4^{con}$) to control for any subtle effects of compound heterozygous inactivation of *Foxd1* and *Smad4*. $Foxd1^{+/Cre}$;

[1]Center for Molecular Medicine, Maine Medical Center Research Institute, Scarborough, ME 04074, USA. [2]Kidney Regenerative Medicine Laboratory, The Rogosin Institute, New York, NY 10065, USA.

*Author for correspondence (leo9022@nyp.org)

L.O., 0000-0002-2825-7663

Handling Editor: Liz Robertson
Received 5 July 2021; Accepted 29 November 2021

Development (2022) 149, dev199984. doi:10.1242/dev.199984

Smad4$^{-/loxp}$ is referred to as *Smad4*^{IC}. In this comparison, the *Smad4*^{IC} group is globally heterozygous for *Smad4*. For this study, we used the *Smad4*$^{tm1Rob/+}$ strain, in which the first coding exon of *Smad4* is removed (Chu et al., 2004). *Smad4*^{con} mice did not develop any overt phenotypes. *Smad4*^{IC} mice were distinguishable from *Smad4*^{con} littermates at birth because they had kinked tails, and they developed hindlimb paralysis during the first postnatal week. These phenotypes are most likely explained by expression of *Foxd1* in the somite and in the central nervous system (Hatini et al., 1994; Robinton et al., 2019). To avoid confounding effects of hindlimb paralysis on postnatal kidney development, analyses were carried out at embryonic time points up to postnatal day (P) 1.

To evaluate the efficiency of Cre recombination, we first compared *Smad4* transcript levels, and found that they are reduced by approximately 60% in *Smad4*^{IC} kidneys versus *Smad4*^{con} (Fig. 1A). To measure recombination efficiency specifically in the *Foxd1* lineage, we selected cells expressing the interstitial cell surface marker PDGFRα (Fig. S1A,B), and single-cell genotyped them (Fig. S1C,D). Fig. 1B summarizes the frequency of recombination of interstitial cells in the *Smad4*^{IC} genetic model; 87.1% of cells were recombined at the *Smad4* locus and thus null for *Smad4*.

To determine whether loss of *Smad4* in the *Foxd1*-expressing interstitial cell progenitor affects lineage commitment, we introduced the *Rosa26R* reporter gene. The localization of *Foxd1* lineage cells in the *Smad4*^{IC}*;Rosa26R* strain was indistinguishable from *Smad4*^{con}*;Rosa26R*, and thus we conclude that lineage commitment is unperturbed (Fig. S2). Transverse sections were cut through the center of the kidney to reveal the cortex and medulla. The cortex contains glomeruli, whereas the medulla does not. The medulla is divided into an outer medulla directly adjacent to the cortex and an inner medulla or papilla that extends into the pelvis of the kidney. For clarity, we refer to three distinct regions: cortex, outer medulla, and papilla (equivalent to inner medulla). Compared with *Smad4*^{con}, *Smad4*^{IC} showed abundant stroma in the outer medulla and papilla, and a paucity of epithelial structures in both of these zones (Fig. 1C,D). The R26R reporter serves as a helpful marker that can be used in parallel with histological analysis to understand the abundance of *Foxd1* lineage cells. Comparison of *Smad4*^{con} (Fig. 1E-J) and *Smad4*^{IC} (Fig. 1K-P) revealed a marked

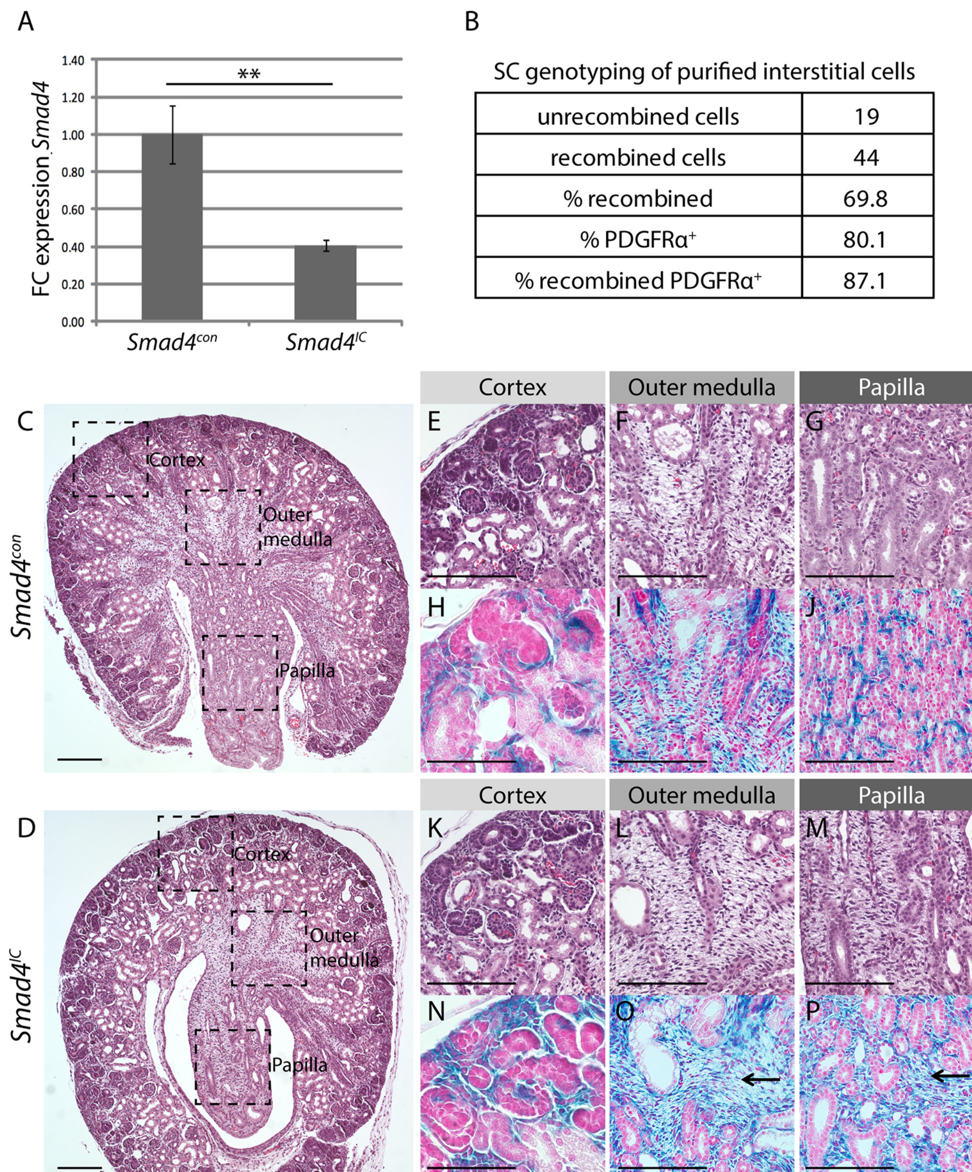

Fig. 1. Single-cell recombination analysis and histology of *Smad4*^{con} and *Smad4*^{IC} postnatal kidneys. (A) *Smad4* transcript levels in whole kidneys isolated from *Smad4*^{con} and *Smad4*^{IC} P0 mice (***P*<0.01; *n*=6). FC, fold change; transcript levels normalized to *Smad4*^{con}±s.e.m. from three separate experiments are plotted. Error bars represent s.e.m. (B) Summary of recombination frequency in purified cortical interstitial cells. (C,D) Transverse kidney sections with boxes showing regions of cortex, outer medulla and papilla shown at higher magnification in E-P. (E-G) Representative H&E fields of *Smad4*^{con} kidneys. (H-J) Representative fields of X-gal-stained sections from kidneys of *Smad4*^{con} on the R26R background. (K-M) Representative H&E fields of *Smad4*^{IC} kidneys. (N-P) Representative fields of X-Gal-stained sections from kidneys of *Smad*^{IC} on the R26R background. Arrows denote X-Gal-positive regions of expanded stroma. Scale bars: 200 µm (C,D); 100 µm (E-P).

expansion of *Foxd1*-lineage interstitium, which was regionalized in the tissue; a modest difference was noted in cortical interstitium (Fig. 1H,N), whereas pronounced pockets of stroma were seen in the outer medulla and papilla (Fig. 1I,J,O,P). We conclude that *Smad4* is required in the *Foxd1* lineage for appropriate formation of the renal interstitium.

Smad4 is required for appropriate differentiation of interstitial cells

During renal development, interstitial cells transition from a FOXD1/PDGFRα double-positive state in the cortex to an α-SMA/PDGFRβ double-positive state in the outer medulla. To determine whether the stromal expansion observed in *Smad4^{IC}* mice is associated with impaired interstitial cell differentiation, expression of the interstitial markers α-SMA and PDGFRβ were examined in kidneys from embryonic and postnatal mice. Though comparable to control at E17.5 (Fig. S3), differences in α-SMA and PDGFRβ expression are observed in *Smad4^{IC}* mouse kidneys by P0. *Smad4^{IC}* mice displayed reduced α-SMA expression in the outer medulla compared with control (Fig. 2A,B). In contrast, PDGFRβ expression was increased in both the outer medulla and papilla of *Smad4^{IC}* mice compared with control (Fig. 2C,D). Confirming these findings, immunoblots of lysates from whole kidneys (Fig. 2E) showed a significant increase of PDGFRβ (Fig. 2F) and decrease of α-SMA (Fig. 2G) in *Smad4^{IC}* mice. The lack of expression of α-SMA in the abundant *Foxd1*-derived interstitial cells of the outer medulla suggests that *Smad4* is required for appropriate expression of their differentiation program.

Loss of Smad4 from the *Foxd1* lineage causes features of collecting duct compression and urine outflow occlusion

One possible explanation for the pockets of interstitial cells seen in the *Smad4^{IC}* medulla is that collecting duct (CD) organization is impaired, causing aberrant clustering of interstitial cells; to determine whether this was the case, we compared *Smad4^{IC}* kidney tissue with controls using two strategies. Three-dimensional modeling of whole kidneys stained with the CD marker TROMA1 (cytokeratin 8) showed that branching at embryonic day (E) 14.5 is indistinguishable between *Smad4^{con}* and *Smad4^{IC}* mice (Fig. 3A-C, Fig. S4A,B). Studies of kidney development using the *Smad4^{tm1Mak}* strain, which has a deletion in the carboxy-terminal domain of SMAD4 (Sirard et al., 1998), have determined a 12% increase in the number of collecting duct branch-points in heterozygotes at E13.5 (Hartwig et al., 2005). The fact that we did not observe any difference between *Smad4^{con}* and *Smad4^{IC}* indicates that this phenotype of global *Smad4* modification is not reproduced with the *Smad4$^{tm1Rob/+}$* strain used in this study. To analyze collecting ducts at P0, when the kidney is too large for modeling based on whole-mount immunostaining, we sectioned through the longitudinal plane of the kidney perpendicular to the papilla to obtain transverse sections of the papilla where collecting ducts are closely bundled (Fig. 3D), and immunostained these sections. We found a reduced number of patent TROMA1-positive structures in the papilla of *Smad4^{IC}* mice compared with *Smad4^{con}* (Fig. 3E,F). High-magnification images of the papilla revealed TROMA1-positive tubules with an atypical, compressed morphology in *Smad4^{IC}* kidneys (Fig. 3G,H). When quantified, the compressed

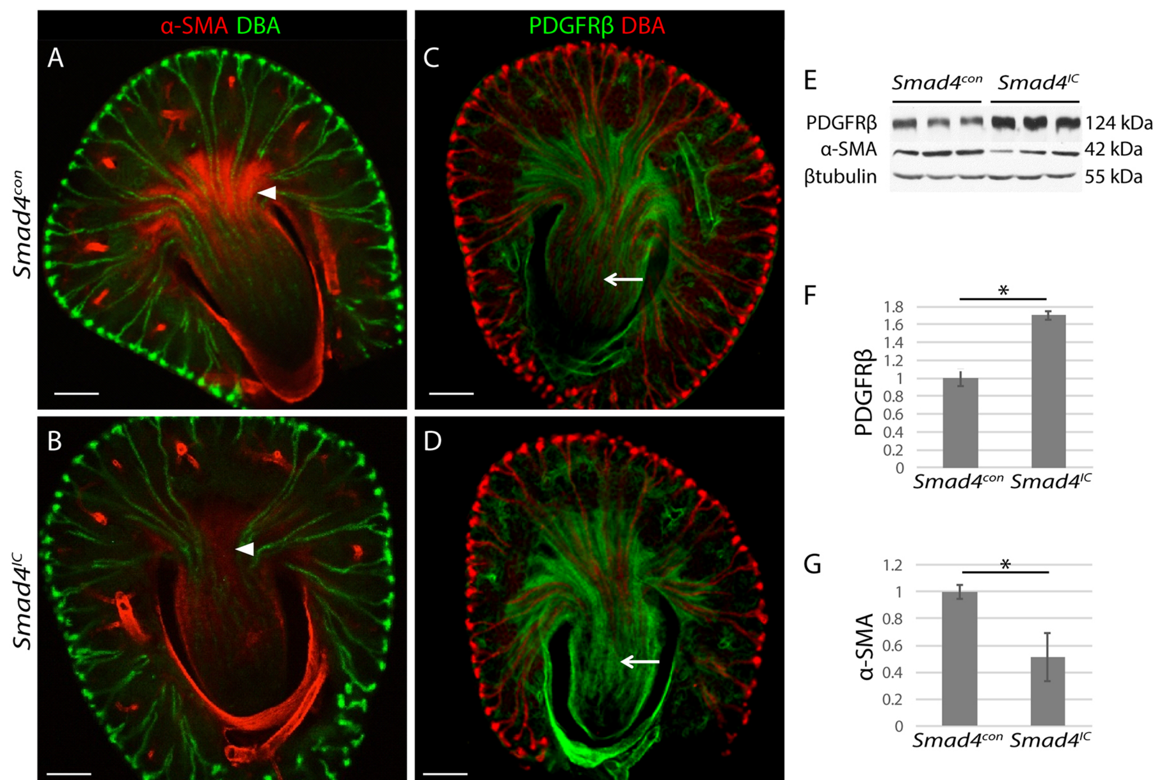

Fig. 2. *Smad4* is required for differentiation of the renal interstitium. (A-D) Whole-mount immunofluorescence of kidney vibratome sections representative of six *Smad4^{con}* and 6 *Smad4^{IC}* kidneys stained with DBA and α-SMA (A,B) or PDGFRβ (C,D) antibodies. Arrowheads mark comparable regions of outer medulla stroma and arrows indicate comparable regions of papillary stroma in *Smad4^{con}* and *Smad4^{IC}*. (E) Immunoblots of whole kidney lysates from three *Smad4^{con}* and three Smad4^{IC} mice probed with α-SMA, PDGFRβ and β-tubulin antibodies. (F,G) Quantification of band intensities for PDGFRβ (F) and α-SMA (G). Error bars are s.e.m. and represent three independent experiments. *P<0.05. Scale bars: 200 µm.

Development (2022) 149, dev199984. doi:10.1242/dev.199984

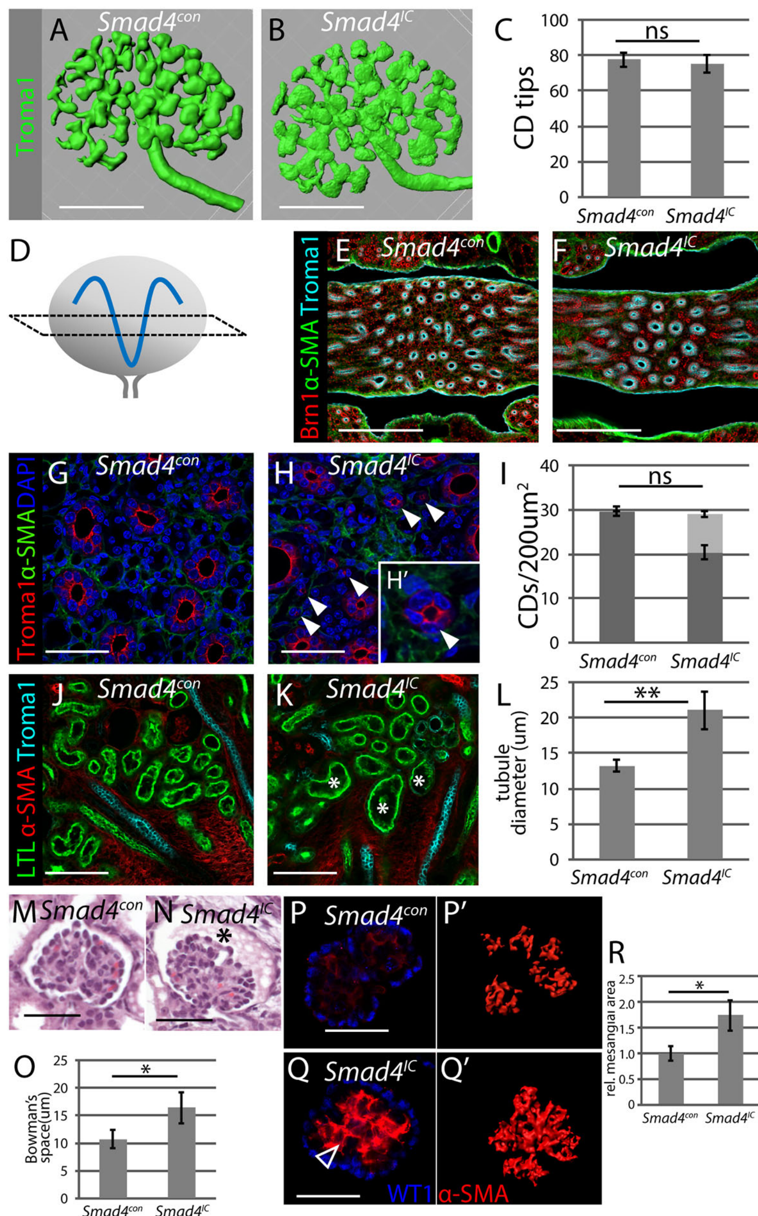

Fig. 3. Interstitial expansion results in collecting duct constriction, tubular distension, and expansion of Bowman's space. (A,B) Three-dimensional reconstruction of E14.5 kidneys from *Smad4*^{con} (A) and *Smad4*^{IC} (B) mice stained for TROMA1. (C) Quantification of collecting duct tip number per E14.5 kidney (*n*=6). (D) Schematic of sectioning plane used for P0 collecting duct analysis. (E,F) P0 kidney vibratome sections stained with Brn1, α-SMA and TROMA1 antibodies. (G-H′) P0 kidney vibratome sections stained with α-SMA and TROMA1 antibodies and DAPI. Arrowheads mark abnormally dimensioned TROMA1^{+} collecting ducts. H′ shows high-magnification image of collecting duct with constricted lumen. (I) Quantification of collecting ducts per 200 µm^2 papilla (*n*=6). Dark gray denotes TROMA1-stained tubules with clearly patent lumens, whereas light gray denotes TROMA1-stained tubules with lumens that are not visibly patent. (J,K) P0 kidney vibratome sections stained with LTL, α-SMA and TROMA1 antibodies. Asterisks mark distended proximal tubules. (L) Quantification of LTL^{+} proximal tubule diameter (*n*=6). (M,N) Representative sections of glomeruli. Asterisk denotes distended Bowman's space. (O) Quantification of Bowman's space from six individual kidneys of each genotype. Only glomeruli that were sectioned through the center were counted. (P,Q) Representative sections through P0 glomeruli co-stained with WT1 and α-SMA antibodies. Arrowhead marks increased mesangial α-SMA expression. (P′,Q′) Maximal intensity projections of *z*-stacks through glomeruli immunostained with α-SMA. (R) Relative mesangial area normalized to *Smad4*^{con} (µm^2; *n*=6) glomeruli. Error bars represent s.e.m. ns, not significant. *P<0.05; **P<0.01. CD, collecting duct. Scale bars: 200 µm (A,B,E,F); 50 µm (G,H,J,K); 20 µm (M,N,P,Q).

TROMA1-expressing CDs account for the reduced number of CDs in *Smad4*^{IC} mice (Fig. 3I). We hypothesize that these structures are remnants of functional CDs that are constricted by stromal expansion. CD compression is predicted to cause restricted urine outflow, and, consistent with this, *Smad4*^{IC} mutant kidneys displayed nephron tubule expansion (Fig. 3J-L) and distended Bowman's spaces (Fig. 3M-O). Increased mesangial α-SMA expression (Fig. 3P-Q′, Fig. S4C,D) and mesangial area (Fig. 3R) indicate early glomerulosclerosis in *Smad4*^{IC} mice. *In vivo* 5-ethynyl-2′-deoxyuridine (EdU) incorporation revealed an increased proliferative index in mesangial cells of the mutant at P0 (Fig. S4E-G), indicating that this defect is mesangioproliferative. Numbers of glomeruli were comparable between *Smad4*^{con} and *Smad4*^{IC} (Fig. S4H), suggesting that the features of increased physiological load that we observed are not due to differences in nephron number. In summary, the histological features that we observed are consistent with CD compression causing increased luminal pressure in the nephron with associated sclerosis of the glomerulus.

Loss of Smad4 affects nuclear accumulation of Smad3 but not Smad1/5/8

To understand whether loss of *Smad4* affects nuclear accumulation of R-Smads in regions of medullary interstitial cell expansion, protein localization of Smads was compared in *Smad4*^{con} and *Smad4*^{IC} mouse kidneys. To localize expression in interstitial cells, we co-stained for α-SMA. Signal amplification was used to detect α-SMA reliably in the *Smad4*^{IC} kidney. After testing multiple different antibodies for receptor Smads, we concluded that nuclear localization of Smad3 is the most sensitive proxy for TGFβ signaling and pSmad1/5/8 is the most sensitive for BMP. These assays are not directly comparable with each other because one measures localization of total protein and the other measure localization of a phosphorylated form. However, signal intensity for each is well documented to correlate with cell signaling, leading us to conclude that they are valid reporters for TGFβ and BMP signaling, respectively. As anticipated, Smad4 was lost from the interstitium of *Smad4*^{IC} mice (Fig. 4A-B′). In addition, Smad3 was strongly reduced in the interstitium of *Smad4*^{IC} kidneys compared

DEVELOPMENT

Development (2022) 149, dev199984. doi:10.1242/dev.199984

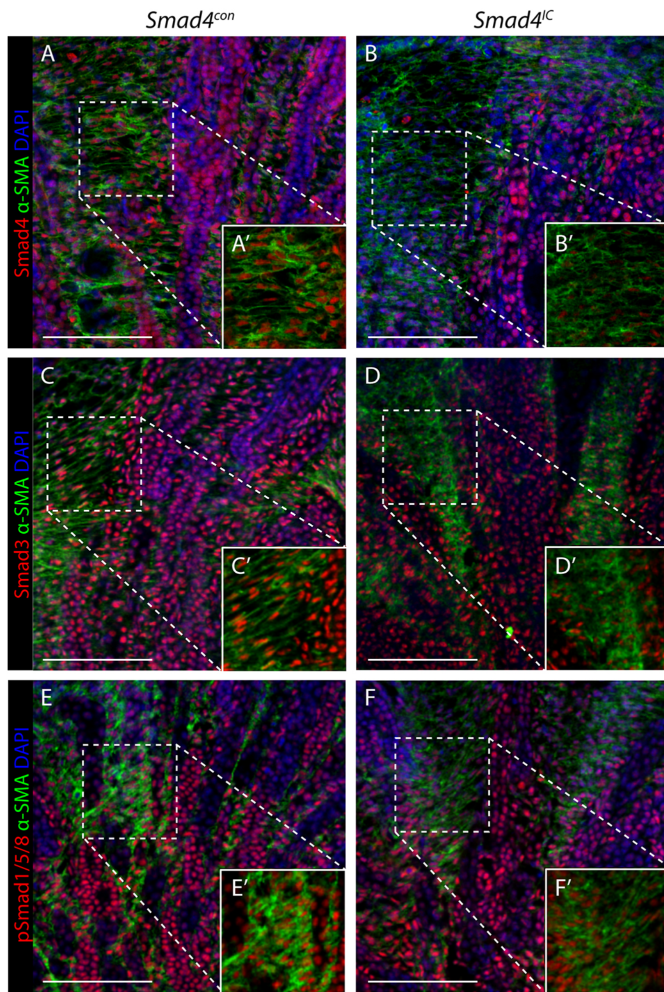

Fig. 4. Nuclear Smad3, but not Smad1/5/8, is decreased in the interstitium of *Smad4^IC^* mice. (A-F′) Immunofluorescence with tyramide signal amplification of P0 kidneys from *Smad4^con^* (A,A′,C,C′,E,E′) and *Smad4^IC^* (B, B′,D,D′,F,F′) mice stained with antibodies recognizing α-SMA (green) and Smad4 (A-B′), Smad3 (C-D′) or pSmad1/5/8 (E-F′); *n*=6. Counterstained with DAPI (blue). Scale bars: 100 μm.

with control (Fig. 4C-D′), whereas pSmad1/5/8 levels were only slightly reduced (Fig. 4E-F′). These results reveal that TGFβ signaling is primarily affected by *Smad4* inactivation.

Smad4^{IC} kidneys are comparable to *Smad4^{con}* at E17.5 but show a phenotype in the newborn, so we were interested to understand whether there were dynamic changes in the TGFβ pathway at late developmental time points. A developmental time course of gene expression in the kidney has been reported (Challen et al., 2005), and we screened developmental time points from E15.5 to P0 for components of the TGFβ signaling pathway. We based the selection of pathway genes on the KEGG pathway hsa04350, which includes 91 genes. Of these, 14 were differentially expressed in the kidney developmental time course. From this transcriptomic analysis, there was no obvious evidence for a coordinated change in the expression of TGFβ pathway components as an equivalent number of genes were up- and downregulated between E17.5 and P0 (Fig. S5).

Interstitial expansion is due to increased proliferation

To determine whether aberrant proliferation is responsible for the interstitial expansion observed in *Smad4^{IC}* mice, we performed *in vivo* EdU incorporation at P0 (Fig. 5). To localize proliferating cells in the interstitium, we co-stained tissue with a cocktail of antibodies for α-SMA and PDGFRβ. These two interstitial cell markers differ strongly in expression level between *Smad4^{IC}* and *Smad4^{con}*, and by detecting both primary antibodies with secondary antibodies conjugated to the same fluorophore we were able to achieve a comparable signal intensity between the two genotypes. Whereas EdU^{+} cycling interstitial cells were largely limited to the cortex and outer medulla in *Smad4^{con}* kidneys, they were abundant in the papilla of *Smad4^{IC}* mice (Fig. 5A-B′). Three-dimensional modeling and quantification of comparable volumes confirmed a higher proliferation rate in the papillary interstitium of *Smad4^{IC}* mice compared with *Smad4^{con}* (Fig. 5C-E). We conclude that there is a failure of interstitial cell growth restriction in the transition zone between the outer medulla and papilla.

Interstitial expansion correlates with aberrant Wnt/β-catenin signaling

Several lines of evidence indicate that Wnt/β-catenin signaling is required for interstitial cell maintenance: loss of *Wnt7B* from the collecting duct epithelium or inactivation of β-catenin in interstitial cell precursors both result in medullary hypoplasia (Boivin et al., 2016; Yu et al., 2009). Thus, developmental genetic studies support a model in which collecting duct-derived Wnt drives medullary interstitial cell proliferation through a β-catenin-dependent signaling mechanism. We were therefore curious to understand whether Wnt/β-catenin signaling was perturbed in the *Smad4^{IC}* kidney. Expression of the feedback inhibitor axin 2 is a sensitive read-out of Wnt/β-catenin signaling, and we compared its expression level in *Smad4^{con}* and *Smad4^{IC}* kidneys. *In situ* hybridization revealed axin 2 expression in the interstitium of the outer medulla and papilla of *Smad4^{con}*, but undetectable levels in *Smad4^{IC}* (Fig. 6A,B, Fig. S6). Reduction in activation of feedback inhibitors can be interpreted as evidence of reduced Wnt/β-catenin signaling, which would be unanticipated considering the proliferative phenotype of *Smad4^{IC}*. We therefore evaluated expression of a panel of other Wnt/β-catenin targets. LEF1 was elevated in the outer medulla and papillary interstitium of *Smad4^{IC}* kidneys (Fig. 6C-E), along with the Wnt/β-catenin-activated cell cycle regulator CCND1 (Fig. 6F-H), suggesting an increase in Wnt/β-catenin signaling and proliferation relative to *Smad4^{con}*. We also found increased expression of the Wnt-responsive cell cycle regulator CDKN1C (p57Kip2) (Fig. 6I-K), which is required for renal medulla formation (Yu et al., 2009; Zhang et al., 1997).

DISCUSSION

Considering the central role that *Smad4* plays in TGFβ superfamily signaling, it is not surprising that the *Foxd1^{IC}* strain displays a profound phenotype in the neonate. TGFβ superfamily signaling in kidney fibroblasts has mainly focused on the study of TGFβ ligands, because foundational work showed that they promote proliferation (Roberts et al., 1985), extracellular matrix deposition (Edwards et al., 1987; Ignotz and Massagué, 1986) and myofibroblast transition (Rønnov-Jessen and Petersen, 1993). In previous work, we explored the consequences of inactivating the TGFβ/MAPK pathway in interstitial cells by inactivating TGFβ-associated kinase 1 (*Map3k7*) using *Foxd1$^{+/Cre}$* (Karolak et al., 2018). In this study, we define the consequences of inactivating the TGFβ/Smad response by inactivating *Smad4*.

TGFβ superfamily ligands promote phosphorylation of the R-Smads 1, 2, 3 and 5 (Ramachandran et al., 2018; Zhang et al., 1996), and therefore one tractable strategy for studying Smad responses is to inactivate *Smad4*, which is required for nuclear

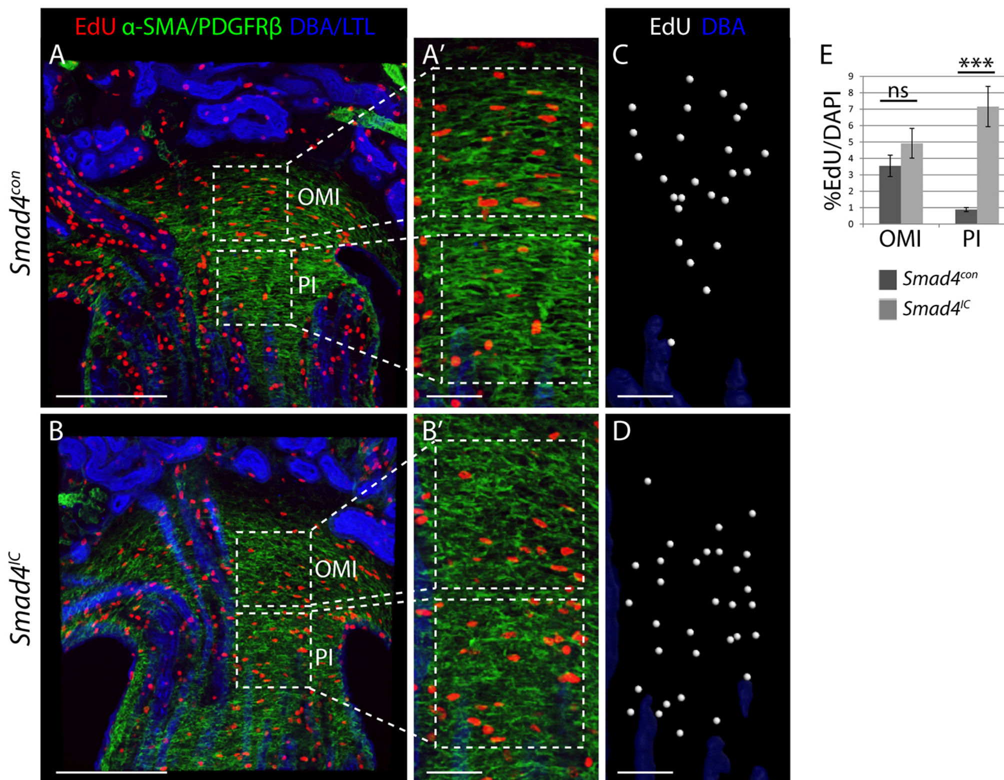

Fig. 5. Loss of *Smad4* leads to increased interstitial proliferation. (A-B′) EdU labeling of kidney sections co-stained with the collecting duct marker DBA, the proximal tubule marker LTL, and α-SMA/PDGFRβ from *Smad4*^{con} (A,A′) and *Smad4*^{IC} (B,B′) mice. (C,D) Three-dimensional tissue analysis of EdU^{+} cells in hatched volumes of the outer medullary interstitium (OMI) and papillary interstitium (PI) using Imaris software. (E) Quantification of three-dimensional analysis showing the percentage of EdU^{+}/DAPI^{+} interstitial cells in the hatched volumes of OMI and IMI of *Smad4*^{con} and *Smad4*^{IC} mice; n=6. Error bars represent s.e.m. ns, not significant. ***P<0.001. Scale bars: 200 µm (A,B); 50 µm (A′,B′,C,D).

retention and transcriptional activity of activated R-Smads (Lagna et al., 1996; Schmierer and Hill, 2005). Unexpectedly, we find that *Smad4* inactivation eliminates nuclear accumulation of the Smad3 transcription factor, but only slightly reduces nuclear accumulation of the Smad1/5 transcription factors. This is in line with the Smad transcriptional response to TGFβ1, which is estimated to comprise approximately 75% Smad2/3 transcriptional response and 25% Smad1/5 transcriptional response (Ramachandran et al., 2018). The finding that Smad1/5 nuclear accumulation is not lost indicates that the BMP R-Smad response is only marginally affected by *Smad4* inactivation. Thus, from the perspective of Smad activation, our genetic model reflects the effects of eliminating TGFβ rather than BMP signaling.

The number of interstitial cells in the kidney must be carefully balanced both during development and in the adult. In development, interstitial cells provide essential signals that guide differentiation of the surrounding epithelia (Das et al., 2013; Fetting et al., 2014). In the adult, interstitial cells provide essential endocrine functions, such as erythropoietin production (Kobayashi et al., 2016), but their uncontrolled expansion is the basis for organ fibrosis whereby functional tissue is marginalized (Humphreys et al., 2010). Our observation that reducing TGFβ/Smad signaling in the interstitial cell lineage leads to increased proliferation in the neonate agrees with findings from studies of multiple cell lines showing that growth is inhibited by TGFβ (Roberts et al., 1985). An interesting feature of our study is that the effect is limited to a particular zone of interstitial cells at the border between the outer medulla and the papilla. Genetic studies have suggested that formation of the medullary interstitium requires Wnt/β-catenin signaling and our work indicates that TGFβ/Smad signaling inhibits this proliferative stimulus in a regional manner to ensure appropriate structural differentiation of the medulla. Interestingly, the effect of knocking out the Wnt/β-catenin pathway in the interstitial lineage is loss of the kidney medulla, but the cortex of these kidneys is preserved (Boivin and Bridgewater, 2018; Yu et al., 2009), suggesting specificity of Wnt/β-catenin for medullary interstitium. Similarly, our inactivation study of *Smad4* reveals overproliferation of the medullary interstitium, indicating that this Wnt/β-catenin–TGFβ/Smad circuit for growth control primarily affects this region.

Loss of *Smad4* causes differential effects on Wnt/β-catenin targets, with a loss of expression of the Wnt feedback inhibitor axin 2 and increased LEF1 and p57Kip2. This supports a model in which loss of feedback inhibition causes increased Wnt/β-catenin signaling resulting in increased proliferation. We hypothesize that the loss of feedback inhibition could be a primary event in the deregulation of interstitial cell proliferation. Multiple Wnts, including *Wnt4* and *Wnt7b*, are expressed in the medullary interstitium (Yu et al., 2009), facilitating combinatorial effects. TGFβ sources have been less well studied, but review of the GenePaint *in situ* hybridization database shows *Tgfb1* expression in the medulla (https://gp3.mpg.de/; Visel et al., 2004). Recent single-cell expression analysis of E18.5 kidneys has shown a spatial intersection of Lef1 expression with expression of the TGFβ-induced transcript *Tgfb1i1*, supporting a model in which Wnt/β-catenin mediated proliferation may be controlled by TGFβ (England et al., 2020). Relative amplitudes of these different signaling pathways could be regulated at the level of the ligands or perhaps more likely by other intracellular signaling components or distinct signaling pathways.

In summary, our findings suggest that Smads and Wnt/β-catenin antagonistically control cell proliferation in the medullary interstitium and that the balance of these signaling pathways determines interstitial cell abundance in the postnatal kidney. Understanding this molecular crosstalk will not only contribute important concepts to the pathogenesis of CAKUT, but may also identify therapeutically tractable mechanisms that control kidney fibrosis in the adult.

Development (2022) 149, dev199984. doi:10.1242/dev.199984

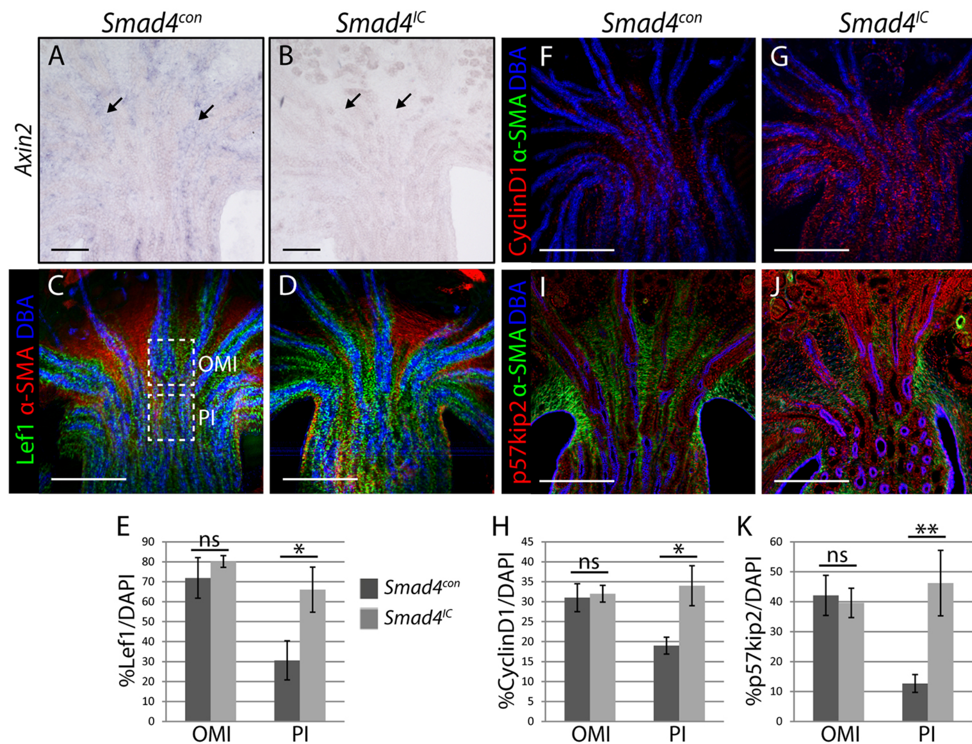

Fig. 6. Increased proliferation is associated with aberrant Wnt signaling. (A,B) Axin 2 *in situ* hybridization on P0 kidneys from *Smad4*^{con} (A) and *Smad4*^{IC} (B) mice. Arrows indicate comparable regions of stroma. (C,D,F,G,I,J) Immunofluorescence staining of vibratome sections of P0 kidneys from *Smad4*^{con} (C,F,I) and *Smad4*^{IC} (D,G,J) mice stained with antibodies recognizing α-SMA and DBA combined with either LEF1 (C,D), cyclin D1 (F,G) or p57Kip2 (I,J). (E,H,K) Quantification of numbers of stained cells in the outer medullary interstitium (OMI) and papillary interstitium (PI) of sections immunostained for LEF1^{+}/DAPI^{+} (E; *n*=6), cyclin D1^{+}/DAPI^{+} (H; *n*=6) or p57Kip2^{+}/DAPI^{+} (K; *n*=6). Examples of regions selected for quantification are shown in C. Error bars represent s.e.m. ns, not significant. **P*<0.05; ***P*<0.01. Scale bars: 200 μm in A-J.

MATERIALS AND METHODS

Mouse strains

Animal care was in accordance with the National Research Council Guide for the Care and Use of Laboratory Animals and protocols were approved by the Institutional Animal Care and Use Committee of Maine Medical Center. The second exon that includes the transcriptional start site is targeted in *Smad4*$^{tm1Rob/+}$ (referred to as *Smad4*$^{+/-}$) and *Smad4*$^{tm1.1Rob/tm1.1Rob}$ (referred to as *Smad4*$^{loxP/loxP}$) mice (Chu et al., 2004). *Foxd1*$^{+/Cre}$;*Smad4*$^{-/+}$ mice were crossed to *Smad4*$^{loxp/loxp}$ mice to produce *Foxd1*$^{+/Cre}$;*Smad4*$^{+/loxp}$ (*Smad4*^{con}) and *Foxd1*$^{+/Cre}$;*Smad4*$^{-/loxp}$ (*Smad4*^{IC}) mice. *Foxd1*$^{+/Cre}$; *Smad4*$^{-/+}$ and *Smad4*$^{loxp/loxp}$ mice were maintained on an ICR background. *R26RlacZ* mice were maintained on an FVB/NJ background.

Reagents

A complete list of antibodies including source, clone name, product number and application are listed in Table S1.

Immunoblotting

Total protein was extracted from whole kidneys as previously described (Blank et al., 2009). Immunoblotting was performed using standard procedures. Antibodies used were anti-α-SMA (1:1000), anti-PDGFRβ (1:1000), anti-Smad4 (1:1000) and anti-β-tubulin (1:5000) (see Table S1). Protein levels were quantified using Fiji/ImageJ software by measuring the integrated density of the indicated proteins normalized to the β-tubulin loading control.

Whole-mount immunofluorescence

E14.5 and P0 kidneys were fixed in 4% paraformaldehyde (PFA) at room temperature for 10 or 30 min, respectively, then transferred to 70% ethanol at −20°C for storage. P0 kidneys were longitudinally or transversely vibratome-sectioned at 100 μm directly into 70% ethanol. Whole kidneys and kidney sections were rehydrated in PBS then permeabilized with 1% Triton X-100 in PBS for 10 min at 4°C. Tissue was washed with PBS to remove residual detergent then incubated in blocking solution (0.01% Tween in PBS plus 5% serum of secondary antibody species) for 1 h. Lectins Dolichos Biflorus Agglutinin (DBA; Vector Laboratories) and Lotus Tetragonolobus Lectin (LTL; Vector Laboratories) were diluted 1:200 and primary antibodies anti-α-SMA-Cy3, anti-PDGFRβ, anti-cytokeratin8/TROMA1, anti-LEF1, anti-BRN1, anti-AnnexinA2, p57Kip2, anti-cyclin D1 and anti-Ki67 (see Table S1) were diluted 1:50 in blocking solution. A Tyramide Signal Amplification kit (TSA; Perkin Elmer) was used according to the manufacturer's protocol for whole-mount immunostaining with anti-Smad4 (1:500), anti-Smad3 (1:3000) and anti-pSmad1/5/8 (1:1000) antibodies (see Table S1). Blocked tissue was incubated in diluted lectins/primary antibodies for 24 h at 4°C followed by three washes with blocking solution, the third wash for 24 h at 4°C. Alexa Fluor 488/568/647 secondary antibodies (Molecular Probes) were used at 1:200 and incubated for 24 h followed by three washes with 0.01% Tween in PBS, the third wash for 24 h at 4°C. Tissue was counterstained with DAPI (1:5000), dehydrated in ethanol, and cleared with BABB (1:1 benzyl alcohol:benzyl benzoate) before imaging with a laser-scanning confocal microscope (Leica Microsystems SP8).

In situ hybridization

P0 kidneys were fixed in 4% PFA overnight at 4°C, washed with PBS for 4 h, then equilibrated in 30% sucrose in PBS overnight at 4°C. After flash-freezing in OCT, kidneys were cryosectioned at 20 μm and sections were fixed in 4% PFA for 10 min, rinsed three times with PBS, incubated in 20 μg/ml proteinase K in PBS for 10 min, followed by three rinses with PBS. Sections were incubated in 1.3% triethalamine and 0.375% acetic anhydride for 10 min, rinsed three times with PBS then incubated in hybridization buffer for 2 h. Digoxigenin (DIG)-labeled axin 2 sense versus antisense riboprobes (Jho et al., 2002) were diluted to 500 ng/ml in hybridization buffer (50% formamide, 5× SSC pH 4.5, 1% SDS, 50 μg/ml yeast tRNA, 50 μg/ml heparin) and sections were hybridized in a humidified chamber at 68°C overnight. After two washes with 0.2× SSC for 30 min at 72°C, sections were rinsed with NTT (0.15 M NaCl, 0.1% Tween-20, 0.1 M Tris-HCl pH 7.5), incubated in blocking buffer (5% heat-inactivated sheep serum, 2% blocking reagent in NTT) for 2 h, followed by incubation in anti-DIG AP-conjugated antibody (diluted 1:4000 in blocking buffer) overnight at 4°C. After three washes with NTT for 30 min each, sections were rinsed with NTTML (0.15 M NaCl, 0.1% Tween-20, 0.1 M Tris-HCl pH 9.5, 50 mM $MgCl_2$, 2 mM levamisole) then incubated in BM Purple until desired staining was reached. Stained sections were rinsed three times with PBS then mounted in glycerol for imaging.

In vivo proliferation analysis

One EdU pulse (20 mg/kg) was administered to P0 pups by intraperitoneal injection. After 2 h, kidneys were dissected on ice and fixed in 4% PFA for 30 min. Kidneys were vibratome sectioned and whole-mount immunofluorescence staining was performed as described above. Click-iT chemistry was subsequently performed on sections according to the manufacturer's protocol (Thermo Fisher) followed by imaging with a laser-scanning confocal microscope (Leica Microsystems SP8). EdU quantification was performed with Imaris image analysis software (Bitplane). Briefly, equivalent 250×250×50 μm^3 image areas were selected in the outer medulla and papilla and the spot function was used to count EdU^+ nuclei. A filter was applied to the spot function to select for PDGFRβ/α-SMA-labeled interstitial cells. Equivalent image analysis, including identical thresholding, was performed on six biological replicates (n=6).

Histology and detection of β-galactosidase activity

Paraffin-embedding and Hematoxylin and Eosin (H&E) staining of tissue was performed by the Maine Medical Center Research Institute Histomorphometry Core. For X-gal staining, whole P0 kidneys were vibratome sectioned (300 µM), rinsed in X-gal buffer (5 mM EGTA; 2 mM $MgCl_2$; 0.02% NP40; 250 µM sodium deoxycholate in PBS) then fixed for 30 min (1% formaldehyde; 0.2% glutaraldehyde in X-gal buffer). Sections were subjected to two 10 min washes with X-gal buffer then stained (5 mM K_3Fe; 5 mM K_4Fe; 0.5 mg/ml X-gal in X-gal buffer) overnight at 37°C. Stained sections were washed twice (10 min each) with X-gal buffer then dehydrated through a series of ethanol/xylene. Dehydrated sections were embedded in paraffin then re-sectioned at 10 µm and counter stained with Nuclear Fast Red.

Single-cell recombination analysis

Nephrogenic zone cells were isolated from E17.5 *Smad4*^{IC} mice as previously described (Brown et al., 2015) and labeled with phycoerythrin (PE)-conjugated anti-mouse CD140a/PDGFRα (1:10; 103-102-502, Miltenyi) followed by incubation with anti-PE MicroBeads (1:20; 130-048-801, Miltenyi). Labeled cells were purified by three rounds of magnetic-activated cell sorting and single cells were manually picked from the PE-positive fraction with the aid of an EVOS FL digital microscope. Total DNA was amplified from single cells with the REPLI-g Single Cell Kit (QIAGEN) and genotyping was performed with NovaTaq Hot Start Master Mix (Millipore) according to the manufacturer's cycling parameters (Tm=55°C) and the primers listed in Table S2.

Statistical analysis

Chi-square testing was performed to verify that all data sets were normally distributed. Two-tailed t-tests were performed comparing normally distributed groups with P>0.05 considered significant. Proliferation analysis of FH535-treated mice and FH535-treated monolayer cells were subject to one-way ANOVA. Asterisks indicate statistical significance as follows: not significant (ns), P>0.05; *P<0.05; **P<0.01; ***P<0.001.

Acknowledgements
The authors gratefully acknowledge Dr Volkhard Lindner for providing the pSmad1/5/8 antibody and the MMCRI Histomorphometry Core for tissue processing and H&E and CD31 staining. The authors also thank Drs Lucy Liaw, Calvin Vary, Pradeep Sathyanaryana and Ron Korstanje for their critical review of this manuscript.

Competing interests
The authors declare no competing or financial interests.

Author contributions
Conceptualization: L.O.; Methodology: S.S.M., M.K., L.O.; Validation: L.O.; Formal analysis: S.S.M., L.O.; Investigation: S.S.M., M.K., L.O.; Resources: L.O.; Data curation: S.S.M., M.K., L.O.; Writing - original draft: S.S.M., L.O.; Writing - review & editing: L.O.; Visualization: S.S.M., L.O.; Supervision: L.O.; Project administration: L.O.; Funding acquisition: L.O.

Funding
The project described was supported by the National Institutes of Health (R24DK106743 and RC2DK125960 to L.O., and F31DK112602 to S.S.M.). Deposited in PMC for release after 12 months.

References

Blank, U., Brown, A., Adams, D. C., Karolak, M. J. and Oxburgh, L. (2009). BMP7 promotes proliferation of nephron progenitor cells via a JNK-dependent mechanism. *Development* **136**, 3557-3566. doi:10.1242/dev.036335

Boivin, F. J. and Bridgewater, D. (2018). β-catenin in stromal progenitors controls medullary stromal development. *Am. J. Physiol. Renal Physiol.* **314**, F1177-F1187. doi:10.1152/ajprenal.00282.2017

Boivin, F. J., Sarin, S., Dabas, P., Karolak, M., Oxburgh, L. and Bridgewater, D. (2016). Stromal β-catenin overexpression contributes to the pathogenesis of renal dysplasia. *J. Pathol.* **239**, 174-185. doi:10.1002/path.4713

Brown, A. C., Muthukrishnan, S. D., Guay, J. A., Adams, D. C., Schafer, D. A., Fetting, J. L. and Oxburgh, L. (2013). Role for compartmentalization in nephron progenitor differentiation. *Proc. Natl. Acad. Sci. U.S.A.* **110**, 4640-4645. doi:10.1073/pnas.1213971110

Brown, A. C., Muthukrishnan, S. D. and Oxburgh, L. (2015). A synthetic niche for nephron progenitor cells. *Dev. Cell* **34**, 229-241. doi:10.1016/j.devcel.2015.06.021

Challen, G., Gardiner, B., Caruana, G., Kostoulias, X., Martinez, G., Crowe, M., Taylor, D. F., Bertram, J., Little, M. and Grimmond, S. M. (2005). Temporal and spatial transcriptional programs in murine kidney development. *Physiol. Genomics* **23**, 159-171. doi:10.1152/physiolgenomics.00043.2005

Chu, G. C., Dunn, N. R., Anderson, D. C., Oxburgh, L. and Robertson, E. J. (2004). Differential requirements for Smad4 in TGFβ-dependent patterning of the early mouse embryo. *Development* **131**, 3501-3512. doi:10.1242/dev.01248

Das, A., Tanigawa, S., Karner, C. M., Xin, M., Lum, L., Chen, C., Olson, E. N., Perantoni, A. O. and Carroll, T. J. (2013). Stromal-epithelial crosstalk regulates kidney progenitor cell differentiation. *Nat. Cell Biol.* **15**, 1035-1044. doi:10.1038/ncb2828

Dudley, A. T., Lyons, K. M. and Robertson, E. J. (1995). A requirement for bone morphogenetic protein-7 during development of the mammalian kidney and eye. *Genes Dev.* **9**, 2795-2807. doi:10.1101/gad.9.22.2795

Edwards, D. R., Murphy, G., Reynolds, J. J., Whitham, S. E., Docherty, A. J., Angel, P. and Heath, J. K. (1987). Transforming growth factor beta modulates the expression of collagenase and metalloproteinase inhibitor. *EMBO J.* **6**, 1899-1904. doi:10.1002/j.1460-2075.1987.tb02449.x

England, A. R., Chaney, C. P., Das, A., Patel, M., Malewska, A., Armendariz, D., Hon, G. C., Strand, D. W., Drake, K. A. and Carroll, T. J. (2020). Identification and characterization of cellular heterogeneity within the developing renal interstitium. *Development* **147**, dev190108. doi:10.1242/dev.190108

Fetting, J. L., Guay, J. A., Karolak, M. J., Iozzo, R. V., Adams, D. C., Maridas, D. E., Brown, A. C. and Oxburgh, L. (2014). FOXD1 promotes nephron progenitor differentiation by repressing decorin in the embryonic kidney. *Development* **141**, 17-27. doi:10.1242/dev.089078

Hartwig, S., Hu, M.-C., Cella, C., Piscione, T., Filmus, J. and Rosenblum, N. D. (2005). Glypican-3 modulates inhibitory Bmp2-Smad signaling to control renal development in vivo. *Mech. Dev.* **122**, 928-938. doi:10.1016/j.mod.2005.03.007

Hartwig, S., Bridgewater, D., Di Giovanni, V., Cain, J., Mishina, Y. and Rosenblum, N. D. (2008). BMP receptor ALK3 controls collecting system development. *J. Am. Soc. Nephrol.* **19**, 117-124. doi:10.1681/ASN.2007010080

Hatini, V., Tao, W. and Lai, E. (1994). Expression of winged helix genes, BF-1 and BF-2, define adjacent domains within the developing forebrain and retina. *J. Neurobiol.* **25**, 1293-1309. doi:10.1002/neu.480251010

Hatini, V., Huh, S. O., Herzlinger, D., Soares, V. C. and Lai, E. (1996). Essential role of stromal mesenchyme in kidney morphogenesis revealed by targeted disruption of Winged Helix transcription factor BF-2. *Genes Dev.* **10**, 1467-1478. doi:10.1101/gad.10.12.1467

Humphreys, B. D., Lin, S.-L., Kobayashi, A., Hudson, T. E., Nowlin, B. T., Bonventre, J. V., Valerius, M. T., McMahon, A. P. and Duffield, J. S. (2010). Fate tracing reveals the pericyte and not epithelial origin of myofibroblasts in kidney fibrosis. *Am. J. Pathol.* **176**, 85-97. doi:10.2353/ajpath.2010.090517

Ignotz, R. A. and Massagué, J. (1986). Transforming growth factor-β stimulates the expression of fibronectin and collagen and their incorporation into the extracellular matrix. *J. Biol. Chem.* **261**, 4337-4345. doi:10.1016/S0021-9258(17)35666-1

Ikeya, M., Fukushima, K., Kawada, M., Onishi, S., Furuta, Y., Yonemura, S., Kitamura, T., Nosaka, T. and Sasai, Y. (2010). Cv2, functioning as a pro-BMP factor via twisted gastrulation, is required for early development of nephron precursors. *Dev. Biol.* **337**, 405-414. doi:10.1016/j.ydbio.2009.11.013

Inazaki, K., Kanamaru, Y., Kojima, Y., Sueyoshi, N., Okumura, K., Kaneko, K., Yamashiro, Y., Ogawa, H. and Nakao, A. (2004). Smad3 deficiency attenuates renal fibrosis, inflammation,and apoptosis after unilateral ureteral obstruction. *Kidney Int.* **66**, 597-604. doi:10.1111/j.1523-1755.2004.00779.x

Jho, E.-H., Zhang, T., Domon, C., Joo, C.-K., Freund, J.-N. and Costantini, F. (2002). Wnt/beta-catenin/Tcf signaling induces the transcription of Axin2, a negative regulator of the signaling pathway. *Mol. Cell. Biol.* **22**, 1172-1183. doi:10.1128/MCB.22.4.1172-1183.2002

Karolak, M. J., Guay, J. A. and Oxburgh, L. (2018). Inactivation of MAP3K7 in FOXD1-expressing cells results in loss of mesangial PDGFRBeta and juvenile kidney scarring. *Am. J. Physiol. Renal Physiol.* **315**, F336-f344. doi:10.1152/ajprenal.00493.2017

Kobayashi, H., Liu, Q., Binns, T. C., Urrutia, A. A., Davidoff, O., Kapitsinou, P. P., Pfaff, A. S., Olauson, H., Wernerson, A., Fogo, A. B. et al. (2016). Distinct

subpopulations of FOXD1 stroma-derived cells regulate renal erythropoietin. *J. Clin. Invest.* **126**, 1926-1938. doi:10.1172/JCI83551

Kohl, S., Hwang, D.-Y., Dworschak, G. C., Hilger, A. C., Saisawat, P., Vivante, A., Stajic, N., Bogdanovic, R., Reutter, H. M., Kehinde, E. O. et al. (2014). Mild recessive mutations in six Fraser syndrome-related genes cause isolated congenital anomalies of the kidney and urinary tract. *J. Am. Soc. Nephrol.* **25**, 1917-1922. doi:10.1681/ASN.2013101103

Lagna, G., Hata, A., Hemmati-Brivanlou, A. and Massagué, J. (1996). Partnership between DPC4 and SMAD proteins in TGF-β signalling pathways. *Nature* **383**, 832-836. doi:10.1038/383832a0

Morishita, Y., Yoshizawa, H., Watanabe, M., Ishibashi, K., Muto, S., Kusano, E. and Nagata, D. (2014). siRNAs targeted to Smad4 prevent renal fibrosis in vivo. *Sci. Rep.* **4**, 6424. doi:10.1038/srep06424

Oxburgh, L., Chu, G. C., Michael, S. K. and Robertson, E. J. (2004). TGFβ superfamily signals are required for morphogenesis of the kidney mesenchyme progenitor population. *Development* **131**, 4593-4605. doi:10.1242/dev.01324

Ramachandran, A., Vizán, P., Das, D., Chakravarty, P., Vogt, J., Rogers, K. W., Müller, P., Hinck, A. P., Sapkota, G. P. and Hill, C. S. (2018). TGF-β uses a novel mode of receptor activation to phosphorylate SMAD1/5 and induce epithelial-to-mesenchymal transition. *eLife* **7**, e31756. doi:10.7554/eLife.31756

Roberts, A. B., Anzano, M. A., Wakefield, L. M., Roche, N. S., Stern, D. F. and Sporn, M. B. (1985). Type β transforming growth factor: a bifunctional regulator of cellular growth. *Proc. Natl. Acad. Sci. USA* **82**, 119-123. doi:10.1073/pnas.82.1.119

Robinton, D. A., Chal, J., Lummertz da Rocha, E., Han, A., Yermalovich, A. V., Oginuma, M., Schlaeger, T. M., Sousa, P., Rodriguez, A., Urbach, A. et al. (2019). The Lin28/let-7 pathway regulates the mammalian caudal body axis elongation program. *Dev. Cell* **48**, 396-405.e393. doi:10.1016/j.devcel.2018.12.016

Rønnov-Jessen, L. and Petersen, O. W. (1993). Induction of alpha-smooth muscle actin by transforming growth factor-beta 1 in quiescent human breast gland fibroblasts. Implications for myofibroblast generation in breast neoplasia. *Lab. Investig.* **68**, 696-707.

Schmierer, B. and Hill, C. S. (2005). Kinetic analysis of Smad nucleocytoplasmic shuttling reveals a mechanism for transforming growth factor β-dependent nuclear accumulation of Smads. *Mol. Cell. Biol.* **25**, 9845-9858. doi:10.1128/MCB.25.22.9845-9858.2005

Sirard, C., de la Pompa, J. L., Elia, A., Itie, A., Mirtsos, C., Cheung, A., Hahn, S., Wakeham, A., Schwartz, L., Kern, S. E. et al. (1998). The tumor suppressor gene Smad4/Dpc4 is required for gastrulation and later for anterior development of the mouse embryo. *Genes Dev.* **12**, 107-119. doi:10.1101/gad.12.1.107

Visel, A., Thaller, C. and Eichele, G. (2004). GenePaint.org: an atlas of gene expression patterns in the mouse embryo. *Nucleic Acids Res*. **1**, D552-D556. doi:10.1093/nar/gkh029

Weber, S., Taylor, J. C., Winyard, P., Baker, K. F., Sullivan-Brown, J., Schild, R., Knüppel, T., Zurowska, A. M., Caldas-Alfonso, A., Litwin, M. et al. (2008). SIX2 and BMP4 mutations associate with anomalous kidney development. *J. Am. Soc. Nephrol.* **19**, 891-903. doi:10.1681/ASN.2006111282

Yu, J., Carroll, T. J., Rajagopal, J., Kobayashi, A., Ren, Q. and McMahon, A. P. (2009). A Wnt7b-dependent pathway regulates the orientation of epithelial cell division and establishes the cortico-medullary axis of the mammalian kidney. *Development* **136**, 161-171. doi:10.1242/dev.022087

Zhang, Y., Feng, X.-H., We, R.-Y. and Derynck, R. (1996). Receptor-associated Mad homologues synergize as effectors of the TGF-beta response. *Nature* **383**, 168-172. doi:10.1038/383168a0

Zhang, P., Liégeois, N. J., Wong, C., Finegold, M., Hou, H., Thompson, J. C., Silverman, A., Harper, J. W., DePinho, R. A. and Elledge, S. J. (1997). Altered cell differentiation and proliferation in mice lacking p57KIP2 indicates a role in Beckwith-Wiedemann syndrome. *Nature* **387**, 151-158. doi:10.1038/387151a0